Biosensors and Bioelectronics 70 (2015) 239–245

Contents lists available at ScienceDirect

Biosensors and Bioelectronics

journal homepage: www.elsevier.com/locate/bios

DNA biosensor-based on fluorescence detection of *E. coli* O157:H7 by Au@Ag nanorods

Jiadi Sun [a], Jian Ji [a], Yanqing Sun [b], Mandour H. Abdalhai [a], Yinzhi Zhang [a], Xiulan Sun [a,*]

[a] State Key Laboratory of Food Science and Technology, School of Food Science and Technology, Synergetic Innovation Center of Food Safety and Nutrition, Jiangnan University, Wuxi, Jiangsu 7214122, PR China
[b] School of Physics and Telecommunication Engineering, Shaanxi University of Technology, Hanzhong 723000, PR China

ARTICLE INFO

Article history:
Received 11 December 2014
Received in revised form
2 March 2015
Accepted 3 March 2015
Available online 5 March 2015

Keywords:
Escherichia coli O157:H7
Au@Ag nanorods
Surface enhanced fluorescence DNAsensor

ABSTRACT

A novel DNA sensor for the detection of the *Escherichia coli* O157:H7 (*E. coli* O157:H7) eaeA gene was constructed using surface enhanced fluorescence (SEF). The spacing distance dependence nature of Au@Ag nanorods surface enhanced fluorescence was investigated when the cy3-labled single strand DNA (ssDNA) and the stem-loop DNA probe modified on the nanorods was co-hybridized. The result revealed that the fluorescence intensity reached the maximum value with the spacing distance of about 10 nm between cy3 and the Au@Ag nanorods surface. Based on this result, a fluorescence "ON/OFF" switch for detecting the eaeA gene of *E. coli* O157:H7 was constructed. Under optimal conditions, the DNA sensor produced a linear range from 10^{-17} to 10^{-11} M with a correlation coefficient of 0.9947 and a detection limit of 3.33×10^{-18} M, and was also found to be specific in targeting eaeA. The DNA sensor demonstrated a new strategy of combining eaeA recognition and Au@Ag nanorods for fluorescence signal enhancement, and increased sensitivity in the detection of bacterial specific genes.

1. Introduction

Food and water are vital resources that are highly susceptible to contamination by pathogenic bacteria such as *Escherichia coli* O157: H7 (*E. coli* O157:H7) (Acuna et al., 2012; Alam and Zurek, 2004). Infection of *E. coli* O157:H7 often leads to hemorrhagic colitis and hemolytic uremic syndrome (HUS), and even death, especially in the young and immunocompromised individuals (Barahona et al., 2013). Traditional microbiological methods for the detection of coliforms include plate counting, multiple-tube fermentation, membrane filter and turbidimetry (Le Ru et al., 2011; Lei et al., 2004; Li et al., 2011). These methods are accurate, but are labor intensive and slow, as they require incubation times of 24–48 h. Polymerase chain reaction (PCR) (Gould et al., 2013; Guo et al., 2012), colony culture (Li et al., 2014; Mao et al., 2006), and immunoassay (e.g. enzyme-linked immunosorbent assays (ELISA)) (Jothikumar and Griffiths, 2002; Karmali, 2004) lack in sensitivity. Thus, alternative approaches for the rapid detection of pathogenic *E. coli* O157:H7 are needed.

Due to their enhanced sensitivity, reproducibility, and selectivity, nanomaterials-based biosensors for DNA detection have become a hot topic of research (Pérez-López and Merkoçi, 2011; Sanchez et al., 2009). The method was first used in the quantification and detection of *E. coli* O157:H7 eaeA gene (Savoye et al., 2011; Schroeder et al., 2002), and later developed for other biosensors, namely the nanogene assays (Sen et al., 2011; Sharma et al., 2010).

Fluorescence spectroscopy is now a widespread technique that has been extensively used in various scientific disciplines. These include bioimaging, medical diagnostics and biosensing, where high sensitivity of the fluorescence-related methods is most desirable (Sonntag et al., 2004; Steele et al., 2010), but low quantum yields limit its practical applications, improving fluorescence sensitivity is an important challenge (Tarr et al., 2005; Vidal et al., 2005). Metal surface enhanced fluorescence (SEF), occurring between the intense plasmon-induced electricfield and the excited-state of fluorophores located in close proximity to noble-metal nanostructures, such as the nanorods (NRs) or nano-crosses (Wu et al., 2012; Yang et al., 2010), is used to improve the sensitivity of fluorescence measurements (Welinder-Olsson and Kaijser, 2005; Wijaya and Hamad-Schifferli, 2008).

Gold/silver core–shell NRs (Au@Ag NRs), with their controllable monodispersity and aspect ratio, broad plasmon resonance tunability from near-ultraviolet (UV) to the infrared (IR) range, as well as their much sharper and stronger longitudinal SPR bands than those of gold NRs (Au NRs), have been successfully utilized in different areas, such as solar energy development (Zhao et al.,

* Correspondence to: Jiangnan University, 1800 Lihu Avenue, Wuxi, Jiangsu 214122, China.
E-mail address: sxlzzz@jiangnan.edu.cn (X. Sun).

http://dx.doi.org/10.1016/j.bios.2015.03.009
0956-5663/

2010), near-IR hyperthermia and nonlinear optical imaging (Zhu et al., 2011). However, little has been reported on their application to DNA assay as surface enhanced fluorescence (SEF) substrates.

In this study, we investigated the metal SEF of the cy3 molecule in the proximity of Au@Ag NRs for the rapid detection of *E. coli* O157:H7 eaeA gene by using the base-paring principle and the unique structural feature of DNA. The separating distance between cy3 and Au@Ag NRs could be controlled effectively, and this investigation provided a simple and convenient approach for studying the distance dependence of metal SEF and designing novel biosensors for molecular fluorescence-based measurements. The influence of the size, shape and distribution of the Au@Ag NRs were investigated as well. Based on the above descriptions, a fluorescence "ON/OFF" switch for detecting the eaeA gene of *E.coli* O157:H7 was constructed. The fluorescence signal was in the "ON" state when the cy3-labeled ssDNA was co-hybridized to the stem-loop DNA probe, which was labeled with amino groups functionalizing Au@Ag NRs surface. In the presence of the target molecule (*E. coli* O157:H7 eaeA gene), the ssDNA would undergo conformational structural change that led to a longer spacing distance (more than 10 nm) between the cy3 end of the modified ssDNA and the Au@Ag NRs surface, and the fluorescence signal was in the"OFF" state. On the basis of this strategy, the *E. coli* O157:H7 eaeA gene was used as a target molecule to be detected experimentally. This straightforward low-cost method facilitates the application of fluorescence spectroscopy to the detection of food pathogens.

2. Experimental

2.1. Equipment

UV–vis spectra were obtained on an Arantes Avaspec-2048 UV–vis spectrophotometer. Transmission electron microscopy images were obtained from a JEOL JEM-2100 (HR). Infrared (IR) spectra were obtained with a Fourier transform infrared (FT-IR) spectrometer (FI-IR, NICOLET MEXUS 470, Thermo Electron Corporation). X-Ray Diffraction (XRD) (D8, BRUKER AXS GMBH) and scanning electron microscope (SEM) (S4800, Hitachi) were used. Circular Dichroism (CD) Spectroscopic were achieved by CD (MOS-450 circular dichroism, Biologic) from 200 to 400 nm. Fluorescence spectra were obtained with a fluorescence spectrophotometer (F-7000, Hitachi); the conditions were as follows: Exicitation wavelength, 525 nm; Emission wavelength, 550–700 nm.

2.2. Reagents

Hydrogen tetrachloroaurate trihydrate ($HAuCl_4$; 99%), 5-bromosalicylic acid (> 98.0%), Sodium salicylate (> 98.0%), sodium borohydride ($NaBH_4$, 99%), cetyltrimethylammonium bromide (CTAB), L-ascorbic acid (> 99.5%) and silver nitrate ($AgNO_3$, > 99%), mercaptoundecanoic acid (MUDA), and sodium hydroxide (NaOH) were purchased from Sigma-Aldrich (Shanghai, China). (N-(3-Dimethylaminopropyl)-N'-ethylcarbodiimide hydrochloride) (EDC) and N-hydroxysulfosuccinimide (sulfo-NHS) were achieved from Sigma-Aldrich (Shanghai, China). cy3-labeled ssDNA and their amino groups modified probes, including the complementary strands (*E. coli* O157:H7 eaeA gene) were purchased from Sangon Biotech (Shanghai, China). Ultrapure water (Millipore, Ultrapure Water Purification Systems) was used to prepare all solutions. The following ssDNA in the design of DNAsensor were shown in Table S1.

2.3. Preparation of Au nanorods and Au@Ag nanorods

Au NRs and Au nano-crosses were synthesized using an improved seed mediated growth method (Zhu et al., 2010), and subsequently functionalized via round-trip ligand exchange to modify the surface with carboxyl groups (Wijaya and Hamad-Schifferli, 2008). Au NRs were prepared as follows: First, a 5 mL amount of 0.5 mM $HAuCl_4$ was mixed with 5 mL of 0.1 M CTAB solution. A 0.6 mL portion of fresh 0.01 M $NaBH_4$ was diluted to 1 mL with water and was then injected into the Au(III)-CTAB solution under vigorous stirring. The solution color changed from yellow to brownish-yellow, and the stirring was stopped after 2 min. The seed solution was aged at room temperature for 30 min before use. Second, 0.4556 g CTAB with 0.0136 g 5-bromosalicylic acid was dissolved in 25 mL deionized water (55 °C), the solution was allowed to cool to 30 °C, when 1.8 mL of 4 mM $AgNO_3$ solution was added. The mixture was kept undisturbed at 30 °C for 15 min, after which 25 mL of 1 mM $HAuCl_4$ solution and, if necessary, a small amount of HCl (37 wt % in water, 12.1 M) was added. After that, ascorbic acid (AA) (0.064 M) was added and the solution was under vigorous magnetic stirring for 30 s until the solution became colorless. Finally, 0.8 mL of seed solution was injected into the growth solution. The resultant mixture was stirred for 30 s and left undisturbed at room temperature at 30 °C for 12 h. Au nanocrosses were similarly prepared by substituting 5-bromosalicylic acid for sodium salicylate. The reaction products were isolated by centrifugation at 8500 rpm for 25 min followed by removal of the supernatant. The precipitates were redispersed in 15 mL of water.

Au@Ag NRs was prepared as follows: First, the mixture of 20 mL of 0.05 M CTAB and the 10 mL of prepared Au NRs were under slow magnetic stirring at 27 °C. Secondly, a certain amount (1.25 mL, 2.5 mL, 3.75 mL) of 3 mM $AgNO_3$ and 600 μL 0.064 M AA were added under vigorous magnetic stirring. Finally, 1.2 mL of 0.1 M NaOH was successively injected into the growth solution. All five sets were then shaken vigorously and put in a 27 °C water bath for 12 h. Within several minutes, the color of the solutions changed from light gray to purple, blue and green according to the amount of added Ag^+ ions. Followed by purification, the Au@Ag NRs solution was concentrated to 10 mL with deionized water.

2.4. Modification of Au@Ag nanorods

The Au@Ag NRs were further functionalized with mercaptoundecanoic acid (MUDA) in a ligand exchange reaction. 33 μL of 0.01 M MUDA were added to 3 mL of the prepared Au@Ag NRs solutions every hour under sonication and let it react for 3 h. Then, the MUDA-labeled NRs were separated from the solution by centrifugation at 8500 rpm for 25 min. After the removal of the excess MUDA ligand in the supernatant, the sediment was resuspended in 1 mL milli-Q water.

2.5. Attachment of stem-loop amino-DNA to Au@Ag nanorods

The procedure for the preparation of stem-loop amino-DNA conjugated Au@Ag NRs was adapted from the previously reported paper (Lierop, 2012; Wijaya and Hamad-Schifferli, 2008). Firstly, the 1 mL MUDA-NRs and 1 mL 0.1 M (N-(3-Dimethylaminopropyl)-N'-ethylcarbodiimide hydrochloride) (EDC) solutions were mixed under stirring for 3 h at pH 4.5 to activate the carboxyl groups functionality. Subsequently, 0.1 M aqueous N-hydroxysulfosuccinimide (sulfo-NHS) and 10^{-6} M stem-loop amino-DNA in a 1:2 M ratio were added and left overnight at room temperature. The modified Au@Ag NRs were then purified by centrifugation at 12,000 rpm for 10 min and redispersed in TE buffer (pH 7.4).

2.6. Preparation of Au@Ag metal surface enhanced fluorescence

Seven different number of bases of cy3-ssDNA (300 μL,10^{-6} M) (12,15, 18, 21, 24, 27, 30) (Table S1) were added to a solution of 200 μL of stem-loop amino-DNA assembled Au@Ag NRs, respectively. The mixture was allowed to hybridize in PBS solution (pH 7.4) for 2 h at 37 °C with shaking, and was purified by centrifugation at 12,000 rpm for 10 min and was then dissolved by buffer. The fluorescence intensities could be detected by the fluorescence spectrophotometer. Repeating the above procedure, seven different fluorescence intensities and the maximum data were achieved.

2.7. Fabrication of "ON-OFF" model for detecting the eaeA gene of E. coli O157:H7

Varying amounts of eaeA gene (ranging from 10^{-20} M to10^{-8} M), in a buffer solution (20 mM Tris–HCl, 0.3 M NaCl, 5 mM $MgCl_2$, pH 8.24) were added into every Au@Ag DNA sensor solution to compete with the cy3-ssDNA to hybridize with the amino-DNA modified on the Au@Ag NRs for 2 h at 37 °C and were then centrifuged at 12,000 rpm for 10 min to obtain the supernatant. The amount of cy3-labeled ssDNA that deviated from stem-loop amino-DNA depended on the amount of eaeA gene, subsequently fluorescence was measured with the supernatant by the fluorescence spectrophotometer.

2.8. Determination of the enhancement factor (EF)

The supernatant subtraction method was used to determine the enhancement factor (Zhou et al., 2014). In order to straightforwardly describe the enhancement efficiency, we defined the enhancement factor according to the following equation: ΔFluorescence (a.u.)$=F_{Ag}-F_s/F_{Ag}$. Where F_{Ag} depicted the fluorescence intensity of the fluorophore attached to Au@Ag NRs and F_s was the fluorescence intensity of the unbound cy3-ssDNA after competing with the target DNA.

3. Results and discussion

3.1. Characteristics of Au and Au@Ag nanorods

Au NRs and Au nanocrosses were synthesized through the seed-mediated growth method (Wu et al., 2012) and their transmission electron microscopy (TEM) images were shown in Fig. 1 (A–C). We produced Ag-coated Au NRs as described in the literature (Wu et al., 2012) by adding preformed Au NRs to a coating solution containing Ag^+ ions. The different electron density of Ag and Au made it possible to clearly visualize the Ag layer around the original Au NRs by TEM, as shown in Fig. 1 (D–F). The images revealed the expected differences of the Ag layer thickness and the different size of Au@Ag NRs.

The UV–vis spectra of Au NRs (a–c) and Au@Ag NRs (d–f) was shown in Fig. 2A. The Au NRs exhibited a longitudinal SPR (LSPR) peak at 807 nm,720 nm and a transverse SPR (TSPR) peak at 511 nm, indicating a rod shape of the gold nanoparticles, as was that of the Au nanocrosses (LSPR:640 nm). However, in those Au NRs and Au nanocrosses which were coated with silver, the LSPR peak blue-shifted to 620 nm, 572 nm and 543 nm due to the reduced aspect ratio. Besides, in the short wavelength region, a new peak appeared at 390 nm and the curve bent slightly upward at around 350 nm, which might be attributed to the unsymmetrical structure of the deposited silver layer. It was also shown that the LSPR band of the Au@Ag NRs could be tuned from the visible to the near infrared region of the optical spectrum, similar to that of the Au NRs. Thus, with corners and edges presented on their surfaces and the tunable optical properties, such Ag coated core–shell NRs could serve as excellent candidates for fluorescent applications (Zong et al., 2012). Different size of Au NRs with

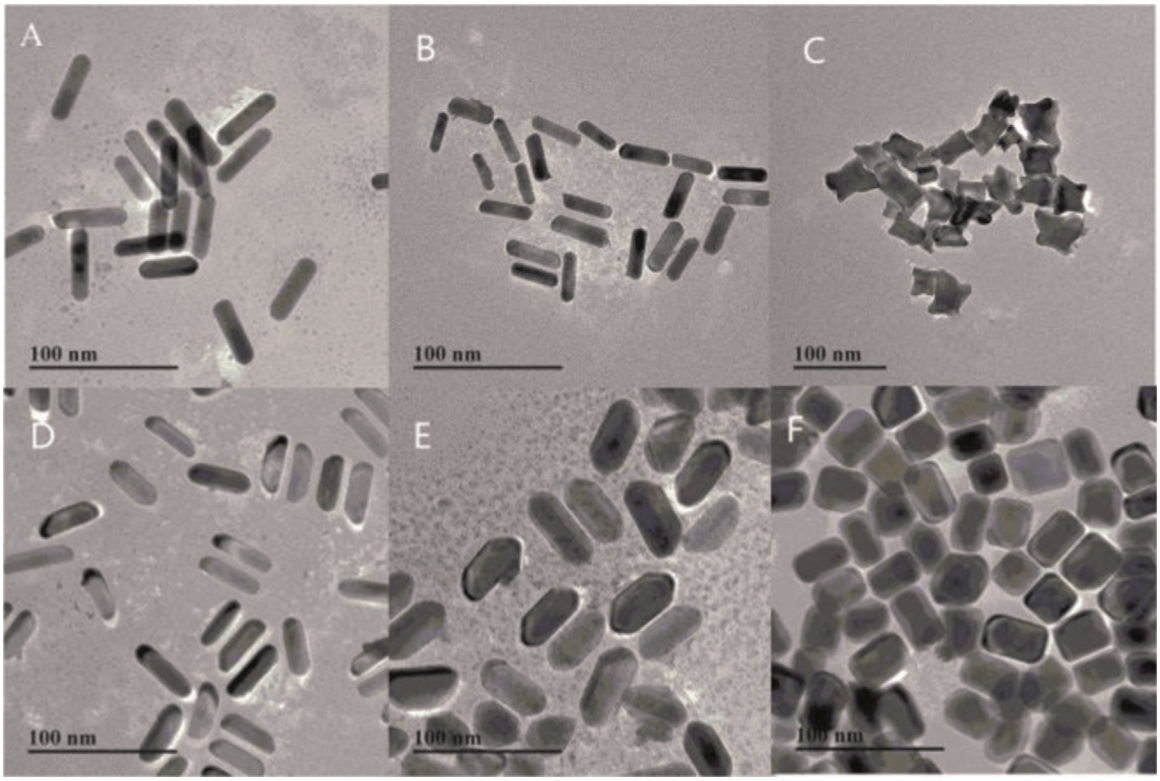

Fig. 1. TEM images of Au nanorods and nanocrosses (A); (B); (C) and Au@Ag nanorods (D); (E); (F).

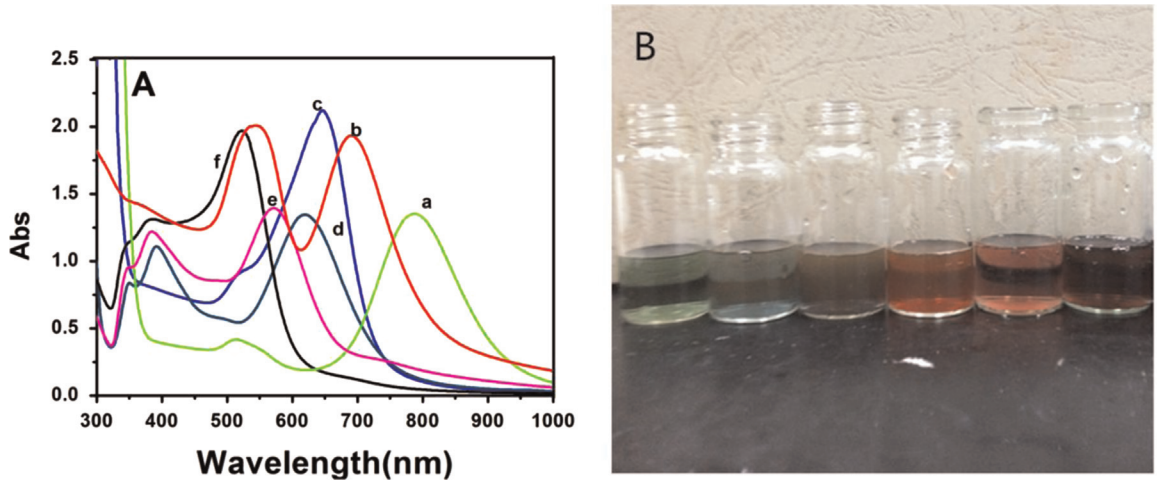

Fig. 2. (A)UV–vis spectra Au nanorods and Au@Ag nanorods and (B) color images of Au nanorods and Au@Ag nanorods.

different amount of added Ag^+ ions in the coating solution led to a strong color shift from red to green (Fig. 2B).

The successful fabrication of Au@Ag NRs could be demonstrated by Energy-dispersive X-ray (EDX) spectrum as shown in Fig. S1. The result indicated that the elements present were C, O, Au, Ag and Cu. The presence of the elements Au and Ag directly confirmed the formation of Au@Ag bimetallic nanoparticles.

High-resolution TEM and X-Ray diffraction analysis (Figs. S2A and B) confirmed the monocrystallinity of the particles and the epitaxial growths of the silver shell on the gold particles; the borders of the Ag shell were indicated by dashed lines. Equal lattice spacing (0.23 nm) in the Au core and the Ag shell confirmed epitaxial growth in the [111] planes, and the two diffraction peaks which appeared at $2\theta = 32^\circ$ and 42°, indicated that the Au@Ag NRs grew mainly in the [111] and [100] planes.

3.2. Characterization of stem-loop amino-DNA assembled Au@Ag nanorods

The stem-loop probe we used, labeled with 5'-NH_2, had been designed such that it had six complementary bases at its 5' (five of them are G–C pairs), so that the DNA strand would be closed by the thermostable G–C pairs to form a stem-loop. The stepwise fabrication process was depicted in Scheme 1. In the absence of the target, the immobilized stem-loop probe was in the "closed" state, when the target was added, it hybridized with the target, and the stem-loop probe was in the "open" state, which favored the formation of the more stable, rigid target-probe duplex. Then the fluorescence intensities could be detected. The stem-loop probe had a great advantage in mismatched discrimination as well.

Au@Ag NRs were found to be well dispersed and did not significantly change in size upon ligand exchange (Fig. S3). The CTAB/5-bromosalicylic acid Au@Ag NRs exhibited absorbance peaks at about 960 cm^{-1}, as a result of the CTAB quaternary amine stretching vibration. Four sharp peaks at 1400–1600 cm^{-1} were attributed to benzene ring stretching vibrations. The MUDA–Au@Ag NRs exhibited peaks at 1600 cm^{-1}, as a result of the MUDA COO-stretching, S–H stretching (2613 cm^{-1}) and C–S stretching (706 cm^{-1}) vibrations, which indicated the synthesis of the MUDA–Au@Ag NRs (Fig. s4).

The stem-loop amino-DNA were conjugated onto the Au@Ag

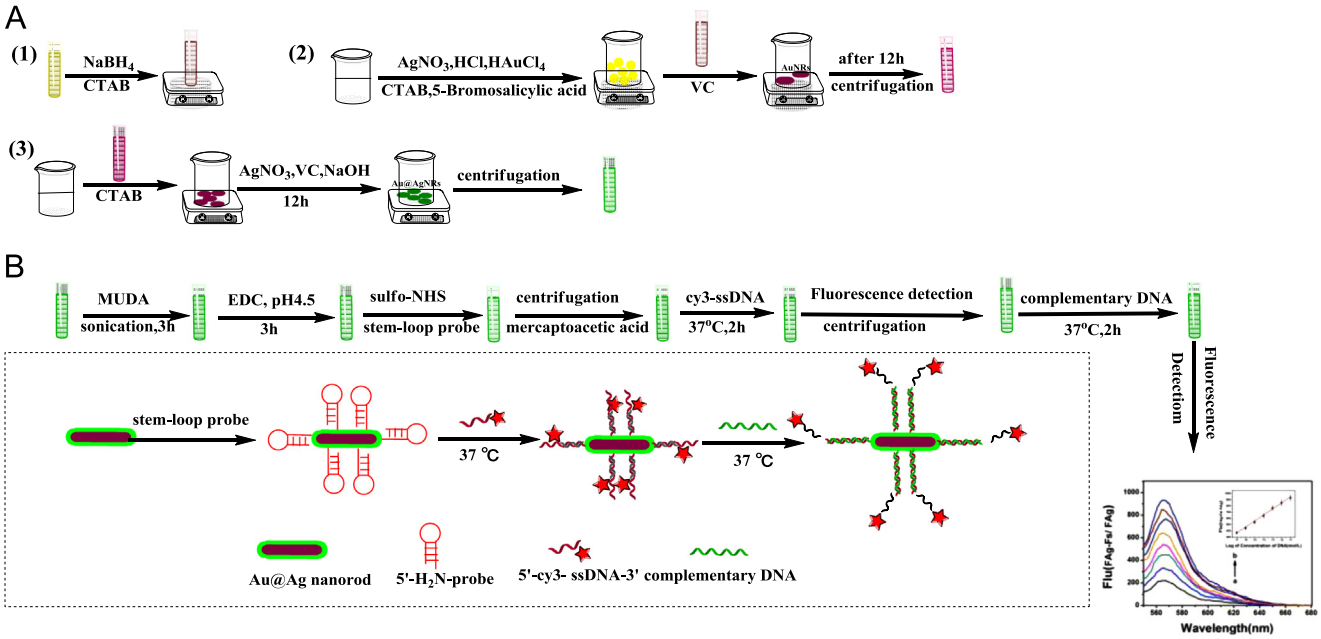

Scheme 1. Schematic illustration of surface enhanced fluorescence DNA sensor using Au@Ag nanorods for the detection of *E. coli* O157:H7 eaeA.

NRs surfaces by the amino-carboxyl reaction, as described in Section 2. The conjugation of Au@Ag with DNA was characterized using UV−vis absorption spectroscopy, and the results were shown in Fig. S5. No changes in the profile were detected and no new peaks appeared in the UV−vis spectrum of carboxyl-functionalized Au@Ag NRs before they were conjugated with stem-loop amine-DNA. After the Au@Ag NRs were incubated with amino-modified DNA and the supernatant was discarded, a new absorption peak appeared at approximately 260 nm, and the position of the peak shifted a little in right direction. The successful coupling of the stem-loop amine-DNA and the carboxyl-functionalized Au@Ag NRs was verified by gel electrophoresis (Fig. S6). Lane 1 represented the 100 bp ssDNA ladder. Low-molecular-weight stem-loop amine-DNA, approximately 40 bp (lane 4), migrated much further compared to the stem-loop amine-DNA−Au@Ag NRs conjugates (lane 2). The differences in the mobility of stem-loop amine-DNA versus stem-loop amine-DNA−Au@Ag NRs conjugates indicated that the amide coupling chemistry was successful, and that the stem-loop amine modified DNA was indeed attached to the surface of the Au@Ag NRs. Additionally, the supernatant separated after the incubation of the stem-loop amine-DNA with the Au@Ag NRs was also analyzed using electrophoresis. A shallow band appeared (lane 3) in the supernatant appeared, which was indicated that the concentration of stem-loop amine-DNA decreased after incubation with Au@Ag NRs.

3.3. Fabrication of "ON" model for enhanced fluorscence

The stem-loop amino-DNA assembled Au@Ag NRs were complemented with the cy3-ssDNA as described above. The mixture of the above stem-loop probe and cy3-ssDNA were kept at 37 °C for 2 h. Then, the cy3-ssDNA, and the mixture at the same amount were each measured by Circular Dichroism (CD) Spectroscopic from 200 to 400 nm. The results in Fig. s7 showed a clear CD profile with two positive peaks at 220 and 270 nm and one negative peak at approximately 250 nm, which indicated that the cy3-ssDNA did possess a definite parallel conformation in solution (curve a). Comparatively, if the cy3-ssDNA were incubated with the probe, the amplitude of the peaks at 220 nm would increase prominently, which most likely indicated an increase in the helicity and folding of the DNA (curve b).

As was shown in Fig. S8, the absorbance of the Au@Ag NRs in solution could overlap with the emission spectral of cy3. Thus we used cy3-labeled ssDNA of different lengths based on the different number of bases complementary with the stem-loop DNA modified on the Au@Ag NRs. Seven ssDNA with different number of bases (12, 15, 18, 21, 24, 27, 30) were chosen and the lengths of the ssDNA were estimated by assuming that the lengths of 3 bases was equivalent to about 1 nm (Huang et al., 2008; Stoermer and Keating, 2006). The fluorescence intensities of these seven different probe-cy3-ssDNA were determined and the maximum fluorescence intensity was obtained from the 30 base pairs of DNA duplex with the cy3 spacing distance of about 10 nm from the Au@Ag NRs surface (Fig. 3).

When the cy3 spacing distance from the Au@Ag NRs surface was either longer or shorter than 10 nm, the fluorescence enhancement response gradually decreased, resulting in decreased fluorescence intensity. This fluorescence intensity response was consistent with that reported for Ag island film.

Fluorescence data indicated that the Au@Ag NRs had the ability of SEF to a certain extent. The reasons were as follows: First, the enhancement of the nonlinear optical effects had a relationship with a narrow ensemble plasmon line width and slope of the plasmon-shape relation connecting the aspect ratio. In other words, coating Au NRs with a thin layer of silver led to a strong reduction of the ensemble linewidth, a desirable feature for most plasmonic applications (Becker et al., 2008), whose LSPR was about 630 nm. Second, the silver shell reduced the plasmon damping due to the higher energy required to excite d-band electrons into the conduction band in Ag compared to Au. The interface between the Au core and the Ag shell apparently caused no additional damping. A smaller single particle linewidth meant lower plasmon damping, thus a longer plasmon lifetime, and the quality factor Q would (relevant for the field enhancement around plasmonic particles) increase for the Ag-coated rods compared to Au rods at the same resonance energy (Jain et al., 2014). Third, if the Ag layer became too thick, the particles started to lose their rodlike shape and the fluorescence enhancement was not obvious, because a slightly thicker Ag layer typically led to more inhomogeneous coating resulting in a broadening of the ensemble linewidth compared to the optimal Ag thickness (Tan et al., 2014) (Fig. S9).

3.4. Fabrication of "OFF" model for enhanced fluorescence

Based on the result of the dependence of enhanced fluorescence intensity on the spacing distance between the cy3 dyes and Au@Ag NRs, a cy3-ssDNA was designed as illustrated in Scheme 1, where the presence and absence of target molecules was equated to an "ON/OFF" switch. In the "OFF" state, the fluorescence signal of the cy3-ssDNA was comparatively lower, which represented the presence of the target molecule. The greater spacing distance happened between the cy3 dye and the Au@Ag NRs surface,

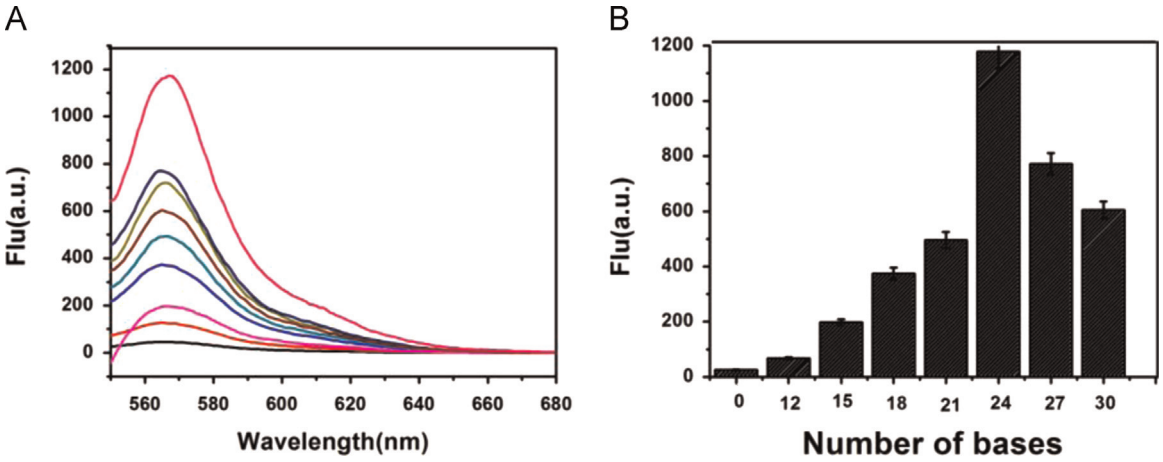

Fig. 3. Fluorescence intensity of different number of bases (12,15, 18, 21, 24, 27, 30) of cy3-ssDNA.

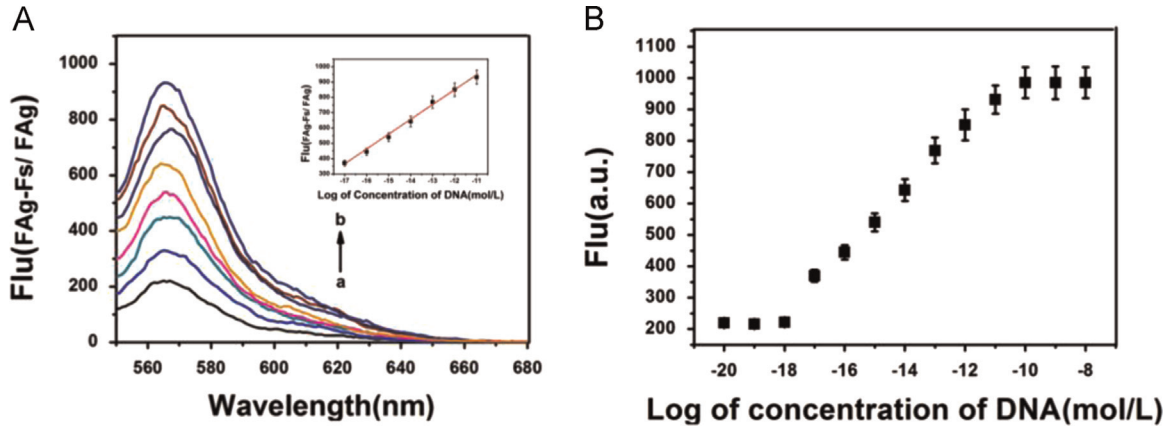

Fig. 4. Standard curves of surface enhanced fluorescence DNA sensor using Au@Ag nanorodss for the detection of *E. coli* O157:H7 eaeA.

because the target molecule competed with the cy3-ssDNA to complement with the probe bind to the Au@Ag nanorods. On the other hand, in the absence of the target molecule, the stem-loop DNA would undergo comformational changes that led to the shortening of the spacing distance between the cy3 dye and the Au@Ag NRs surface. The resulting increase in the fluorescence signal intensity was considered to represent as the "ON" state.

3.5. The optimal condition of DNAsensor

The different volumes of cy3-ssDNA bind to the stem-loop amino-DNA assembled Au@Ag NRs were tested to determine the amount of cy3 dye that yielded optimal results. Fig. S10 showed that the strongest fluorescence intensity was attained with 225 μL of cy3-ssDNA hybridizing with the 200 μL of stem-loop-DNA–Au@Ag NRs. The stem-loop-DNA modified on the Au@Ag NRs were hybridized with the cy3-ssDNA for 10, 20, 30, 40, 50, 60, 70, 80, 90, 100, 110 and 120 min to investigate the dependence of the surface enhanced fluorescence on the hybridization time. The results revealed that a longer hybridization time resulted in a greater intensity of the cy3 dyes. The largest fluorescence enhancement was obtained with a hybridization time of 90 min (Fig. S11), with an enhancement factor of up to 10. Therefore, the optimum hybridization time to prepare the stem-loop-DNA modified on the Au@Ag NRs and the cy3-ssDNA was 90 min.

3.6. Analytical performance

Having determined the optimal assay conditions, the DNA sensor was used to detect varying concentrations of the target eaeA gene (ranging from 10^{-20} to 10^{-8} M) under such conditions. The fluorescent intensities of the fluorophore attached to the Au@Ag NRs was depicted as F_{Ag} and the fluorescence intensity of the unbound cy3-ssDNA after competing with the target DNA was depicted as F_s, thus $F_{Ag}-F_s$ referred to the change of the fluorescence. A plot of the relative fluorescence intensity ($F_{Ag}-F_s/F_{Ag}$) versus the logarithm of the concentration of the eaeA gene gave a linear (Fig. 4) response represented by the equation $y=95.97x+1992.49$ ($R^2=0.9947$). The linear concentration range we observed was from 10^{-17} to 10^{-11} M. The detection limit was 3.33×10^{-18} M, which was comparatively lower than the reported method for detecting *E. coli* eaeA (Table S2).

In order to assess the specificity of the DNA sensor, we compared the relative fluorescence intensity brought by eaeA and other numbers of bases mismatch. The relative fluorescence response ($F_{Ag}-F_s/F_{Ag}$) was found to be much lower for 10^{-11} M eaeA than for those mutated genes with a number of base mismatches under the same experimental conditions (Fig. S12), which suggested that the developed biosensor was very selective. This high selectivity was thought to result in the high specificity of the test for the detection of *E. coli* O157:H7.

3.7. Analytical application

In order to test the capacity of the biosensor to detect the target bacteria in the samples, 10 mL tap water was inoculated with *E. coli* O157:H7 before filtered it through membrane to eliminate the contaminant flora. Then, centrifuging (10,000 rpm for 5 min) it to concentrate the inoculums followed by bacterial genomic DNA extraction, which was then used in a PCR procedure to amplify the target DNA for the direct hybridization detection. The *E. coli* O157:H7 genomic DNA was initially denatured at 95 °C for 3 min, followed by 30 cycles of 30 s denaturation at 95 °C, 30 s annealing at 60 °C, 1 min extension at 72 °C, and 5 min final extension. After amplification, we achieved a concentration of 0.6×10^{-4} mol/L using the Nanodrop platform, and was diluted it 10^{10} times for the test. The newly constructed sensor was used to detect the DNA in the above mentioned samples, from which recoveries were calculated. The *E. coli* eaeA recoveries (Table 1) were in the range of 98.36–101.67%, which indicated the high accuracy of the DNA sensor and its potential for the rapid detection of *E. coli* O157:H7 in water.

4. Conclusion

We investigated the distance dependence nature between the fluorescence dye and the Au@Ag NRs through cy3-labeled ssDNA and a novel structure for switching a biosensor based on the stem-loop amino-DNA modified on the Au@Ag NRs. This DNA sensor

Table 1
Recovery of surface enhanced fluorescence DNA sensor for the detection of *E. coli* O157:H7($n=3$).

Sample	Background concentration (mol L^{-1})	Added concentration (mol L^{-1})	Detected concentration (mean+SD) (mol L^{-1})	Recovery (%)	RSD (%)
E. coli	0.60×10^{-14}	0.62×10^{-14}	$1.20\times10^{-14}+0.01\times10^{-14}$	98.36	0.83
	0.60×10^{-14}	0.58×10^{-14}	$1.17\times10^{-14}+0.001\times10^{-14}$	99.41	0.086
	0.60×10^{-14}	0.60×10^{-14}	$1.22\times10^{-14}+0.01\times10^{-14}$	101.67	1.64

was found to selectively detect the eaeA gene with high sensitivity, while exhibiting a linear response to the eaeA gene concentrations ranging from 10^{-17} to 10^{-11} M and a limit of detection of 3.33×10^{-18} M. This DNA sensor was simple, rapid and low cost. The spacing distance dependence effect of Au@Ag NRs was universal to almost all fluorophores which offered the possibility to design the multicolor nanosensors. Such a nanosensor also had potential application in high-throughput bioassay for small molecules.

Acknowledgements

This work has been supported by National Natural Science Foundation of China (No. 31371768), National research program (No. 201203069), the Program for New Century Excellent Talents in Jiangnan University, Qinglan Project, Synergetic Innovation Center of Food Safety and quality control, and the Priority Academic Program Development of Jiangsu Higher Education Institutions.

Appendix A. Supplementary material

Supplementary data associated with this article can be found in the online version at http://dx.doi.org/10.1016/j.bios.2015.03.009.

References

Acuna, G., Möller, F., Holzmeister, P., Beater, S., Lalkens, B., Tinnefeld, P., 2012. Fluorescence enhancement at docking sites of DNA-directed self-assembled nanoantennas. Science 338 (6106), 506–510.

Alam, M.J., Zurek, L., 2004. Association of *Escherichia coli* O157:H7 with houseflies on a cattle farm. Appl. Environ. Microbiol. 70 (12), 7578–7580.

Barahona, F., Bardliving, C.L., Phifer, A., Bruno, J.G., Batt, C.A., 2013. An aptasensor based on polymer-gold nanoparticle composite microspheres for the detection of malathion using surface-enhanced Raman Spectroscopy. Ind. Biotechnol. 9 (1), 42–50.

Becker, J., Zins, I., Jakab, A., Khalavka, Y., Schubert, O., Sönnichsen, C., 2008. Plasmonic focusing reduces ensemble linewidth of silver-coated gold nanorods. Nano Lett. 8 (6), 1719–1723.

Gould, L.H., Walsh, K.A., Vieira, A.R., Herman, K., Williams, I.T., Hall, A.J., Cole, D., 2013. Surveillance for foodborne disease outbreaks—United States, 1998–2008. MMWR Surveill. Summ. 62 (2), 1–34.

Guo, Z., Nam, S., Park, S., Yoon, J., 2012. A highly selective ratiometric near-infrared fluorescent cyanine sensor for cysteine with remarkable shift and its application in bioimaging. Chem. Sci. 3 (9), 2760–2765.

Huang, Y.-F., Chang, H.-T., Tan, W., 2008. Cancer cell targeting using multiple aptamers conjugated on nanorods. Anal. Chem. 80 (3), 567–572.

Jain, A., Tassin, P., Koschny, T., Soukoulis, C.M., 2014. Large quality factor in sheet metamaterials made from dark dielectric meta-atoms. Phys. Rev. Lett. 112 (11), 117403.

Jothikumar, N., Griffiths, M.W., 2002. Rapid detection of *Escherichia coli* O157: H7 with multiplex real-time PCR assays. Appl. Environ. Microbiol. 68 (6), 3169–3171.

Karmali, M.A., 2004. Prospects for preventing serious systemic toxemic complications of shiga toxin–producing *Escherichia coli* infections using shiga toxin receptor analogues. J. Infect. Dis. 189 (3), 355–359.

Le Ru, E.C., Grand, J., Sow, I., Somerville, W.R., Etchegoin, P.G., Treguer-Delapierre, M., Charron, G., Félidj, N., Lévi, G., Aubard, J., 2011. A scheme for detecting every single target molecule with surface-enhanced Raman spectroscopy. Nano Lett. 11 (11), 5013–5019.

Lei, C.-X., Hu, S.-Q., Gao, N., Shen, G.-L., Yu, R.-Q., 2004. An amperometric hydrogen peroxide biosensor based on immobilizing horseradish peroxidase to a nano-Au monolayer supported by sol–gel derived carbon ceramic electrode. Bioelectrochemistry 65 (1), 33–39.

Li, K., Huang, J., Shi, G., Zhang, W., Jin, L., 2011. A sensitive nanoporous gold-based electrochemical DNA biosensor for *Escherichia coli* detection. Anal. Lett. 44 (16), 2559–2570.

Li, Y., Afrasiabi, R., Fathi, F., Wang, N., Xiang, C., Love, R., She, Z., Kraatz, H.-B., 2014. Impedance based detection of pathogenic *E. coli* O157: H7 using a ferrocene-antimicrobial peptide modified biosensor. Biosens. Bioelectron. 58, 193–199.

Lierop, D., 2012. Positively charged silver nanoparticles and their effect on surface-enhanced Raman scattering of dye-labelled oligonucleotides. Chem. Commun. 48 (66), 8192–8194.

Mao, X., Yang, L., Su, X.-L., Li, Y., 2006. A nanoparticle amplification based quartz crystal microbalance DNA sensor for detection of *Escherichia coli* O157: H7. Biosens. Bioelectron. 21 (7), 1178–1185.

Pérez-López, B., Merkoçi, A., 2011. Nanomaterials based biosensors for food analysis applications. Trends Food Sci. Technol. 22 (11), 625–639.

Sanchez, S., Martinez, R., Alonso, J., Rey, J., 2009. Clinical and pathogenic aspects of infections due to *Escherichia coli* O157: H7 and other verocytotoxigenic *E. coli*. Enferm. Infecc. Microbiol. Clin. 28 (6), 370–374.

Savoye, F., Feng, P., Rozand, C., Bouvier, M., Gleizal, A., Thevenot, D., 2011. Comparative evaluation of a phage protein ligand assay with real-time PCR and a reference method for the detection of *Escherichia coli* O157: H7 in raw ground beef and trimmings. J. Food Prot.® 74 (1), 6–12.

Schroeder, C.M., Meng, J., Zhao, S., DebRoy, C., Torcolini, J., Zhao, C., McDermott, P.F., Wagner, D.D., Walker, R.D., White, D.G., 2002. Antimicrobial resistance of *Escherichia coli* O26, O103, O111, O128, and O145 from animals and humans. Emerg. Infect. Dis. 8 (12), 1409–1414.

Sen, K., Sinclair, L., Boczek, J., Rice, E.W., L., 2011. Development of a sensitive detection method for stressed *E. coli* O157: H7 in source and finished drinking water by culture-qPCR. Environ. Sci. Technol. 45 (6), 2250–2256.

Sharma, J., Yeh, H.-C., Yoo, H., Werner, J.H., Martinez, J.S., 2010. A complementary palette of fluorescent silver nanoclusters. Chem. Commun. 46 (19), 3280–3282.

Sonntag, A.-K., Prager, R., Bielaszewska, M., Zhang, W., Fruth, A., Tschäpe, H., Karch, H., 2004. Phenotypic and genotypic analyses of enterohemorrhagic *Escherichia coli* O145 strains from patients in Germany. J. Clin. Microbiol. 42 (3), 954–962.

Steele, J.M., Gagnidze, I., Wiele, S.M., 2010. Efficient extraction of fluorescence emission utilizing multiple surface plasmon modes from gold wire gratings. Plasmonics 5 (3), 319–324.

Stoermer, R.L., Keating, C.D., 2006. Distance-dependent emission from dye-labeled oligonucleotides on striped Au/Ag nanowires: effect of secondary structure and hybridization efficiency. J. Am. Chem. Soc. 128 (40), 13243–13254.

Tan, Y., Sutanto, E., Alleyne, A.G., Cunningham, B.T., 2014. Photonic crystal enhancement of a homogeneous fluorescent assay using submicron fluid channels fabricated by E-jet patterning. J. Biophoton. 7 (3–4), 266–275.

Tarr, P.I., Gordon, C.A., Chandler, W.L., 2005. Shiga-toxin-producing *Escherichia coli* and haemolytic uraemic syndrome. Lancet 365 (9464), 1073–1086.

Vidal, M., Kruger, E., Durán, C., Lagos, R., Levine, M., Prado, V., Toro, C., Vidal, R., 2005. Single multiplex PCR assay to identify simultaneously the six categories of diarrheagenic *Escherichia coli* associated with enteric infections. J. Clin. Microbiol. 43 (10), 5362–5365.

Welinder-Olsson, C., Kaijser, B., 2005. Enterohemorrhagic *Escherichia coli* (EHEC). Scand. J. Infect. Dis. 37 (6–7), 405–416.

Wijaya, A., Hamad-Schifferli, K., 2008. Ligand customization and DNA functionalization of gold nanorods via round-trip phase transfer ligand exchange. Langmuir 24 (18), 9966–9969.

Wu, L., Wang, Z., Zong, S., Huang, Z., Zhang, P., Cui, Y., 2012. A SERS-based immunoassay with highly increased sensitivity using gold/silver core–shell nanorods. Biosens. Bioelectron. 38 (1), 94–99.

Yang, B., Lu, N., Qi, D., Ma, R., Wu, Q., Hao, J., Liu, X., Mu, Y., Reboud, V., Kehagias, N., 2010. Tuning the intensity of metal-enhanced fluorescence by engineering silver nanoparticle arrays. Small 6 (9), 1038–1043.

Zhao, L., Mei, S., Chu, P.K., Zhang, Y., Wu, Z., 2010. The influence of hierarchical hybrid micro/nano-textured titanium surface with titania nanotubes on osteoblast functions. Biomaterials 31 (19), 5072–5082.

Zhou, Z., Huang, H., Chen, Y., Liu, F., Huang, C.Z., Li, N., 2014. A distance-dependent metal-enhanced fluorescence sensing platform based on molecular beacon design. Biosens. Bioelectron. 52 (0), 367–373.

Zhu, P., Shelton, D.R., Li, S., Adams, D.L., Karns, J.S., Amstutz, P., Tang, C.-M., 2011. Detection of *E. coli* O157:H7 by immunomagnetic separation coupled with fluorescence immunoassay. Biosens. Bioelectron. 30 (1), 337–341.

Zhu, S., Zhang, J., Vegesna, G., Luo, F.-T., Green, S.A., Liu, H., 2010. Highly water-soluble neutral BODIPY dyes with controllable fluorescence quantum yields. Org. Lett. 13 (3), 438–441.

Zong, S., Wang, Z., Yang, J., Wang, C., Xu, S., Cui, Y., 2012. A SERS and fluorescence dual mode cancer cell targeting probe based on silica coated Au@Ag core–shell nanorods. Talanta 97 (0), 368–375.